

# Comparison of three-dimensional Poisson solution methods for particle-based simulation and inhomogeneous dielectrics

Claudio Berti,<sup>1,\*</sup> Dirk Gillespie,<sup>2</sup> Jaydeep P. Bardhan,<sup>2</sup> Robert S. Eisenberg,<sup>2</sup> and Claudio Fiegna<sup>1</sup>

<sup>1</sup>*ARCES, University of Bologna and IUNET, Via Venezia 260, I-47521 Cesena, Italy*

<sup>2</sup>*Department of Molecular Biophysics and Physiology, Rush University Medical Center, Chicago, Illinois 60612, USA*

(Received 7 February 2012; published 12 July 2012)

Particle-based simulation represents a powerful approach to modeling physical systems in electronics, molecular biology, and chemical physics. Accounting for the interactions occurring among charged particles requires an accurate and efficient solution of Poisson's equation. For a system of discrete charges with inhomogeneous dielectrics, i.e., a system with discontinuities in the permittivity, the boundary element method (BEM) is frequently adopted. It provides the solution of Poisson's equation, accounting for polarization effects due to the discontinuity in the permittivity by computing the induced charges at the dielectric boundaries. In this framework, the total electrostatic potential is then found by superimposing the elemental contributions from both source and induced charges. In this paper, we present a comparison between two BEMs to solve a boundary-integral formulation of Poisson's equation, with emphasis on the BEMs' suitability for particle-based simulations in terms of solution accuracy and computation speed. The two approaches are the collocation and qualocation methods. Collocation is implemented following the induced-charge computation method of D. Boda *et al.* [*J. Chem. Phys.* **125**, 034901 (2006)]. The qualocation method is described by J. Tausch *et al.* [*IEEE Transactions on Computer-Aided Design of Integrated Circuits and Systems* **20**, 1398 (2001)]. These approaches are studied using both flat and curved surface elements to discretize the dielectric boundary, using two challenging test cases: a dielectric sphere embedded in a different dielectric medium and a toy model of an ion channel. Earlier comparisons of the two BEM approaches did not address curved surface elements or semiatomistic models of ion channels. Our results support the earlier findings that for flat-element calculations, qualocation is always significantly more accurate than collocation. On the other hand, when the dielectric boundary is discretized with curved surface elements, the two methods are essentially equivalent; i.e., they have comparable accuracies for the same number of elements. We find that ions in water—charges embedded in a high-dielectric medium—are harder to compute accurately than charges in a low-dielectric medium.

DOI: [10.1103/PhysRevE.86.011912](https://doi.org/10.1103/PhysRevE.86.011912)

PACS number(s): 87.15.kr, 41.20.Cv, 87.14.ep

## I. INTRODUCTION

Numerical simulation represents a useful technique to investigate physical systems at the nanoscale level. Although the computational capability of modern supercomputers allows one to perform fully atomistic simulations of larger and larger systems, simpler models are still widely used. Such models, if well formulated and applied, are able to provide great insights with fewer parameters and much less computational effort than their fully atomistic counterparts. One of the most popular coarse-grained techniques treats a reduced number of particles of interest explicitly and uses a potential of mean force (PMF) to account for the effect of all other particles [1–9].

For example, when dealing with a system of charged particles, the primitive or implicit-solvent models describe the effect of water molecules collectively as a dielectric background that mediates electrostatic interactions by dielectric polarization. The inhomogeneous simulation domain is divided into a number of homogeneous regions, each with constant permittivity. This approach is particularly convenient for simulations of ions in electrolytes, because the number of ions is orders of magnitude smaller than the number of solvent molecules, enabling faster computation [3,6,10–17].

This kind of simulation preserves the discrete nature of the ions themselves and, therefore, allows realistic analysis of

their behavior at the atomic level. For example, one can study permeation of ions through membrane pores by dividing the simulation domain into two regions (the membrane and water) and assigning each region its own permittivity. One can then model the motion of the ions in the water regions, neglecting the dynamics of water molecules or membrane atoms except for their electrostatic effects on the ions' motion. This kind of coarse-graining approach is standard practice for simulations of electronic devices [18–24] and has been widely used to investigate solvation of macromolecules [25,26], interacting proteins [27,28], and ion-channel permeation [29–40].

However, this approach requires the evaluation of electrostatic forces in a simulation domain with inhomogeneous dielectrics, which poses serious practical challenges for computation, particularly if one insists on using periodic boundary conditions [41–43]. In particular, to compute the forces on the ions, one must account for the inhomogeneity of the permittivity  $\epsilon(\mathbf{r})$  (here, discontinuities occurring at the boundaries between different materials or phases) by solving Poisson's equation, which relates the source charge distribution  $\rho(\mathbf{r})$  to the electrostatic potential  $\Phi(\mathbf{r})$  in the simulation domain,

$$\epsilon_0 \nabla \cdot [\epsilon(\mathbf{r}) \nabla \Phi(\mathbf{r})] = -\rho(\mathbf{r}), \quad (1)$$

where  $\epsilon_0$  is the permittivity of free space. Solving Poisson's equation is a computationally slow task, especially in

\*cberti@arces.unibo.it

comparison to problems in which the permittivity is constant everywhere, and it is further challenged for periodic systems.

Different approaches have been proposed to solve Poisson's equation in systems with inhomogeneous dielectric permittivity, depending on the specific characteristics of the simulation domain; the most popular are volume-based techniques such as the finite-difference method [44–49], the finite-element method [50–53], and boundary-integral equation methods solved via the boundary element method (BEM) [54–62].

All of these methods lead ultimately to a system of algebraic equations for numerical solution, and the intrinsic properties of the system being studied help to determine the most efficient technique. For example, finite-difference and finite-element methods are well suited for the numerical simulations of electronic devices such as P-N junctions [63,64] and MOSFETs [65,66], where one deals with thousands of charges so they can be described by a position-dependent volume (or surface) density, but one loses the discrete nature of particles. However, finite-difference and finite-element approaches can lead to significant accuracy challenges for simulations of nanometer-scale structures, where the number of charges is typically relatively small or where the charge-charge distances can be comparable to the distance between grid points.

BEM can provide an accurate treatment of electrostatics in nanoscale simulation domains while preserving the discrete nature of the ions. For example, simulations of ions near and within nanometer molecular structures such as ion channels have been performed with a high accuracy with this approach [10,61,67,68].

In this paper we address methods that compute the polarization charges induced on the dielectric interfaces; other BEM approaches calculate the potential or electric field at the interface [69–71]. The induced surface charges are determined as a weighted sum of simple basis functions defined on a grid of surface (boundary) elements that discretize the whole dielectric boundary. This approach does not require discretization of the entire three-dimensional simulation domain; only the two-dimensional boundary surfaces. The weights for the basis functions (i.e., the polarization charge densities) are determined by enforcing the continuity of the electric displacement through the dielectric boundaries. Once the induced charges have been computed, they contribute to the distribution of electrostatic potential in the same way as source charges; thus, the total electrostatic potential (i.e., the solution to Poisson's equation) is explicitly calculated as the Coulomb potential due to the two distributions of charges, the source charges and the induced boundary charges. Thus, BEM is particularly well suited for coarse-grained simulations of primitive-model electrolyte solutions near and within proteins such as ion channels and has been adapted to treat protein/solvent interfaces [67,68,72].

Performing BEM simulations requires careful choice of discretization techniques. It matters how the analytically exact boundary-integral equation is converted into an approximate, finite-dimensional system of algebraic equations. As with other numerical methods, there is a trade-off between speed and accuracy: one obtains better approximations by using more unknowns, but not all discretization methods exhibit the same trade-off. In this paper we compare two approaches to BEM: the induced-charge computation (ICC) centroid collocation

method [61] and the qualocation (QUAL) method [71,73,74]. These two approaches start from the same boundary-integral equation formulation of the Poisson problem [54,57,59], but use different numerical approximations to compute the needed integrals that lead to the BEM matrix equation  $\mathbf{A}\mathbf{h} = \mathbf{b}$ .

Some earlier studies have addressed either simplistic model problems [74] or broader technical questions of discretizing integral equation models [71], but using only flat boundary elements. Curved boundary elements offer much better accuracy for a given number of unknowns [75–77], which makes them of great value for Brownian dynamics (BD) or Monte Carlo (MC) simulations [67,78,79], when speed is especially important due to the large number of matrix operations. Mathematical analysis of the QUAL method suggested that its advantages might not be as large for curved boundary elements. In this paper, we test this hypothesis and found it to be true. We first validate our implementation by confirming the earlier QUAL results showing QUAL's accuracy advantage for flat boundary elements. For curved boundary elements, however, the QUAL and collocation methods exhibit essentially the same accuracy. Finally, our results show the difference between collocation and QUAL is most pronounced when source charges lie in a high dielectric medium, which is consistent with the results of Bardhan *et al.* [74] and Greengard and Lee [80].

## II. THEORY AND METHODS

### A. Boundary element methods

In this section we specify the continuum electrostatic model used to treat discrete charges in an inhomogeneous dielectric domain, and the two BEMs we use to solve the model numerically. We assume a system made of different regions with different permittivities ( $\epsilon_1$  inside and  $\epsilon_2$  outside), separated by a sharp rigid boundary  $\mathcal{B}$ . For any point  $\mathbf{s}$  on  $\mathcal{B}$ , with outward pointing normal  $\mathbf{n}(\mathbf{s})$ , we define

$$\Delta\epsilon = \epsilon_2 - \epsilon_1 \quad (2)$$

$$\bar{\epsilon} = \frac{\epsilon_1 + \epsilon_2}{2} \quad (3)$$

as the change and the mean of dielectric constant as one crosses the boundary. The electric charges of interest (e.g., ions in a solution) are modeled as a set of point charges acting as the sources of the electric field. There are no continuous charge densities and the only source of electric field is a set of point charges. We denote with  $q_k$  and  $\mathbf{r}_k$  the charge and the position of the  $k$ th point charge. This electrostatic problem can be solved using the ICC integral equation [54,61]:

$$\begin{aligned} h(\mathbf{s}) + \frac{\Delta\epsilon}{4\pi\bar{\epsilon}}\mathbf{n}(\mathbf{s}) \cdot \int_{\mathcal{B}} \frac{\mathbf{s} - \mathbf{s}'}{|\mathbf{s} - \mathbf{s}'|^3} h(\mathbf{s}') d\mathbf{s}' \\ = -\frac{\Delta\epsilon}{4\pi\bar{\epsilon}}\mathbf{n}(\mathbf{s}) \cdot \sum_k \frac{q_k}{\epsilon(\mathbf{r}_k)} \frac{\mathbf{s} - \mathbf{r}_k}{|\mathbf{s} - \mathbf{r}_k|^3} \end{aligned} \quad (4)$$

where  $h(\mathbf{s})$  is the induced charge at the dielectric boundary and  $\epsilon(\mathbf{r}_k)$  denotes the permittivity at the location of the  $k$ th fixed charge; for example, if the  $k$ th charge is inside the boundary, we have  $\epsilon(\mathbf{r}_k) = \epsilon_1$ . After solving the boundary-integral equation for the distribution of induced charge  $h(\mathbf{s})$  on the boundary, one can easily evaluate the total electrostatic potential  $\Phi(\mathbf{r})$  at

any point  $\mathbf{r}$  via:

$$\Phi(\mathbf{r}) = \frac{1}{4\pi\epsilon_0} \sum_k \frac{q_k}{\epsilon(\mathbf{r}_k)|\mathbf{r} - \mathbf{r}_k|} + \frac{1}{4\pi\epsilon_0} \int_B \frac{h(\mathbf{s}')}{|\mathbf{r} - \mathbf{s}'|} d\mathbf{s}'. \quad (5)$$

The first and the second terms on the right-hand side of Eq. (5) are the contributions to the electric potential due to the source charges and the charge induced on the dielectric boundary, respectively; the second term is the *reaction potential* because it describes the potential due to the induced surface charge.

### B. Numerical Solution Methods

Linear boundary-integral equations such as Eq. (4) must be solved numerically. Here, approximate solutions for the induced surface charge  $h(\mathbf{s})$  are obtained by introducing a finite number of boundary elements (also called tiles) that partition the boundary  $B$ , or an approximation to it. Introducing a set of piecewise constant basis functions on these boundary elements and using Galerkin projection [81], Eq. (4) is converted into a matrix equation  $\mathbf{A}\mathbf{h} = \mathbf{b}$ . The vector  $\mathbf{b}$  is the right-hand side of Eq. (4). Each entry reflects the normal electric displacement field induced by the fixed charges over the corresponding tile. The matrix  $\mathbf{A}$  accounts for interactions between charge distributions on the individual tiles. The vector  $\mathbf{h}$  consists of the weights for the basis functions on each tile, and thus defines the unknown induced polarization charges. Note that  $\mathbf{A}$  depends only on the conformation and the discretization of the dielectric boundary, and that the vector  $\mathbf{b}$  depends only on the position of the source charges with respect to the boundary elements. After solving for  $\mathbf{h}$ , the induced charge densities over the boundary are known and the electrostatic potential can be found through Eq. (5) by adding the Coulombic contributions from all the charges in the system (source and induced).

According to Bardhan *et al.* [74], the standard Galerkin projection framework [81] for BEM defines the entries of  $\mathbf{A}$  by

$$A_{ij} = \int_{B_i} \left( \delta_{ij} + \int_{B_j} \left( \frac{\Delta\epsilon(\mathbf{s})}{4\pi\bar{\epsilon}(\mathbf{s})} \frac{\mathbf{n}(\mathbf{s}) \cdot (\mathbf{s} - \mathbf{s}')}{|\mathbf{s} - \mathbf{s}'|^3} \right) d\mathbf{s}' \right) d\mathbf{s} \quad (6)$$

and the elements of  $\mathbf{b}$  as

$$b_i = - \int_{B_i} \left( \frac{\Delta\epsilon(\mathbf{s})}{4\pi\bar{\epsilon}(\mathbf{s})} \sum_k \frac{q_k}{\epsilon(\mathbf{r}_k)} \frac{\mathbf{n}(\mathbf{s}) \cdot (\mathbf{s} - \mathbf{r}_k)}{|\mathbf{s} - \mathbf{r}_k|^3} \right) d\mathbf{s}, \quad (7)$$

where  $B_i$  denotes the  $i$ th boundary element and  $\delta_{ij}$  is the Kronecker delta function. The double integrals in Eq. (6) are slow to compute, however, and the focus of this paper is to provide a deeper understanding of two fast approximations to Eqs. (6) and (7).

The *collocation* discretization is by far the more popular, as its derivation is extremely intuitive (e.g., [61,82]). As described by Boda *et al.* [61], the collocation approach to BEM approximates Eqs. (6) and (7) using one-point quadrature for the integrals over each  $B_i$ . The resulting matrix equation can be simplified to obtain a linear system in which each element of  $\mathbf{A}$  takes the form:

$$A_{ij} = \delta_{ij} + \frac{\Delta\epsilon(\mathbf{s}_i)}{4\pi\bar{\epsilon}(\mathbf{s}_i)} \int_{B_j} \frac{(\mathbf{s}_i - \mathbf{s}') \cdot \mathbf{n}(\mathbf{s}_i)}{|\mathbf{s}_i - \mathbf{s}'|^3} d\mathbf{s}', \quad (8)$$

and each element of vector  $\mathbf{b}$  is:

$$b_i = - \frac{\Delta\epsilon(\mathbf{s}_i)}{4\pi\bar{\epsilon}(\mathbf{s}_i)} \sum_k \frac{q_k}{\epsilon(\mathbf{r}_k)} \frac{\mathbf{s}_i - \mathbf{r}_k}{|\mathbf{s}_i - \mathbf{r}_k|^3} \cdot \mathbf{n}(\mathbf{s}_i) \quad (9)$$

where  $\mathbf{s}_i$  is the centroid of the  $i$ th boundary element.

An alternative to collocation is the QUAL method proposed by Tausch [73] and later applied by Bardhan and Altman *et al.* [71,74,83], which (i) changes the order of the double integral of Eq. (6) and then (ii) adopts one-point quadrature to approximate the new outer integral. The elements of  $\mathbf{A}$  then take the form

$$A_{ij} = a_i \delta_{ij} + \frac{\Delta\epsilon(\mathbf{s}_i)}{4\pi\bar{\epsilon}(\mathbf{s}_i)} a_j \int_{B_j} \frac{(\mathbf{s} - \mathbf{s}_j) \cdot \mathbf{n}(\mathbf{s})}{|\mathbf{s} - \mathbf{s}_j|^3} d\mathbf{s}, \quad (10)$$

where  $a_i$  denotes the area of tile  $i$ , i.e.,

$$a_i = \int_{B_i} d\mathbf{s}. \quad (11)$$

Each element of vector  $\mathbf{b}$  becomes

$$b_i = - \frac{\Delta\epsilon(\mathbf{s}_i)}{4\pi\bar{\epsilon}(\mathbf{s}_i)} \int_{B_i} \left( \sum_k \frac{q_k}{\epsilon(\mathbf{r}_k)} \frac{\mathbf{s}' - \mathbf{r}_k}{|\mathbf{s}' - \mathbf{r}_k|^3} \cdot \mathbf{n}(\mathbf{s}') \right) d\mathbf{s}'. \quad (12)$$

Here, we always use a one-point quadrature for the integral in Eq. (12), which has been shown to be sufficiently accurate [74]. The success of one-point quadrature for computing the right-hand side vector  $\mathbf{b}$  contrasts sharply with the complications needed to approximate the matrix  $\mathbf{A}$ . The reason for its success is that the integrands for the entries of  $\mathbf{b}$  are extremely smooth, because charges never get within 1 Å of the tile. In contrast, computing entries of  $\mathbf{A}$  involves computing singular and near-singular integrals:

$$b_i = - \frac{\Delta\epsilon(\mathbf{s}_i)}{4\pi\bar{\epsilon}(\mathbf{s}_i)} a_i \sum_k \frac{q_k}{\epsilon(\mathbf{r}_k)} \frac{\mathbf{s}_i - \mathbf{r}_k}{|\mathbf{s}_i - \mathbf{r}_k|^3} \cdot \mathbf{n}(\mathbf{s}_i). \quad (13)$$

Regardless of the numerical approach employed, however, one must compute integrals over the boundary elements in Eqs. (8), (9), and (12). For elements that are far away from one another, these integrations can be done with simple quadrature rules; however, the task is more challenging for the “self-term,” i.e., the diagonal matrix entries, as well as the “near-term” interactions where the boundary elements  $i$  and  $j$  are close in proximity. The diagonal matrix entries involve computing the integral of a singular function, and those for nearby elements require integration of near-singular functions. Although these integrals are well defined analytically, their numerical approximation by standard quadrature methods can be computationally expensive (requiring many integration points and thus evaluations of the Green’s function  $1/r$ ). For simple flat elements, these integrals have simple and fast analytical representations [84,85], but integration over curved surfaces requires more complicated and specialized treatment [75,76,86,87]. In this work, for consistency we use the same simple but effective scheme for both flat and curved elements; we divide each boundary element, or tile, into subelements (subtiles) and use numerical quadrature over the subtiles. Our results include an exploration of how accuracy changes as one increases the number of subtiles used in integration, providing a verification of these approaches.

There are four steps to solving a BEM matrix equation using LU factorization. First, one must calculate the dense matrix  $\mathbf{A}$ , which takes time proportional to  $N^2$ , where  $N$  is the number of boundary elements. Second, one must calculate the right-hand side  $\mathbf{b}$ , which takes time proportional to  $NM$ , where  $M$  is the number of fixed charges. The third step is the slowest: computing triangular matrices  $\mathbf{L}$  and  $\mathbf{U}$  such that  $\mathbf{A} = \mathbf{LU}$  requires  $N^3$  time. The final step is to apply the inverses of  $\mathbf{L}$  and  $\mathbf{U}$  to obtain  $\mathbf{h} = \mathbf{U}^{-1}\mathbf{L}^{-1}\mathbf{b}$ , which requires  $N^2$  time due to their triangular nature.

Many large-scale BEM calculations employ iterative methods to solve for  $\mathbf{h}$  approximately, for instance, using the GMRES algorithm [88]. Unlike direct methods, iterative approaches do not need all  $N^2$  entries of  $\mathbf{A}$  but only the ability to multiply an arbitrary vector  $\mathbf{x}$  by  $\mathbf{A}$ ; this product can be computed very quickly (time and memory requirements proportional to  $N$  only or to  $N \log N$ ) using techniques such as fast multipole methods [89–91], precorrected FFT [92], or FFTSVD [77,93]. These algorithms are said to be *asymptotically faster* because they will outperform the direct methods for sufficiently large  $N$ ; however, for BD or MC simulations with simple reduced models of ion channels, direct methods can be faster because  $N$  is usually not large.

### C. Gauss's Law as a consistency check

One way to assess the collocation and qualocation methods' performance on a given boundary discretization is to check a sum rule (consistency check) based on Gauss's Law. The sum rule is derived by integrating both sides of Eq. (4) over any closed surface  $\mathcal{B}'$ :

$$\begin{aligned} \int_{\mathcal{B}'} h(\mathbf{s}) d\mathbf{s} + \frac{1}{4\pi} \frac{\Delta\epsilon}{\bar{\epsilon}} \int_{\mathcal{B}'} h(\mathbf{s}') \int_{\mathcal{B}} \frac{\mathbf{n}(\mathbf{s}) \cdot (\mathbf{s} - \mathbf{s}')}{|\mathbf{s} - \mathbf{s}'|^3} d\mathbf{s} d\mathbf{s}' \\ = -\frac{1}{4\pi} \frac{\Delta\epsilon}{\bar{\epsilon}} \sum_k \frac{q_k}{\epsilon_k} \int_{\mathcal{B}'} \frac{\mathbf{n}(\mathbf{s}) \cdot (\mathbf{s} - \mathbf{r}_k)}{|\mathbf{s} - \mathbf{r}_k|^3} d\mathbf{s}, \end{aligned} \quad (14)$$

where we assume for simplicity that there is only one dielectric interface so that  $\Delta\epsilon$  and  $\bar{\epsilon}$  are independent of  $\mathbf{s}$ . By Gauss's Law, the integral on the left-hand side is the Heaviside step

function:

$$\frac{1}{4\pi} \int_{\mathcal{B}'} \frac{\mathbf{n}(\mathbf{s}) \cdot (\mathbf{s} - \mathbf{s}')}{|\mathbf{s} - \mathbf{s}'|^3} d\mathbf{s} = \begin{cases} 1 & \text{if } \mathbf{s}' \text{ is inside } \mathcal{B}', \\ \frac{1}{2} & \text{if } \mathbf{s}' \text{ is on } \mathcal{B}', \\ 0 & \text{if } \mathbf{s}' \text{ is outside } \mathcal{B}'. \end{cases} \quad (15)$$

Therefore,  $h$  must satisfy

$$\left(1 + \frac{1}{2} \frac{\Delta\epsilon}{\bar{\epsilon}}\right) \int_{\mathcal{B}'} h(\mathbf{s}) d\mathbf{s} = -\frac{\Delta\epsilon}{\bar{\epsilon}} \sum_{k \in \mathcal{B}'} \frac{q_k}{\epsilon_k}, \quad (16)$$

where the sum on the right-hand side is over the charges inside  $\mathcal{B}'$ .

To gauge the electrostatic self-consistency of our calculations, we define

$$h_{\text{tot}} = -\epsilon_q \left( \frac{1}{2} + \frac{\bar{\epsilon}}{\Delta\epsilon} \right) \int_{\mathcal{B}'} h(\mathbf{s}) d\mathbf{s}, \quad (17)$$

where we have assumed that all the source charges are in one dielectric  $\epsilon_q$ . Then a measure of how well the sum rule, Eq. (16) is satisfied is how close  $h_{\text{tot}}$  is to  $\sum_k q_k$ .

## III. RESULTS

Throughout this section we use the notations ICC and QUAL and remind the reader that these are not different underlying *models*, merely different numerical approaches to solving the same model. We employ two challenging test cases to compare the ICC and QUAL methods: first, a single point charge in a spherical dielectric [Fig. 1(a)] and, second, a simple model of a protein ion channel [Figs. 1(b) and 1(c)]. The first case, thanks to the availability of an exact analytical solution, provides general and rigorous insights about the accuracy of the two methods; we studied the complementary problems of a high-dielectric sphere in a low-dielectric medium and of a low-dielectric sphere in a high-dielectric medium. The ion-channel test case offers a more meaningful measure of the methods' ability to describe electrostatics in a real application, e.g., BD or MC simulations. Thus, to compare the accuracy of ICC and QUAL, we computed the reaction potential induced by a cation along three trajectories through the channel.

For all test cases, we compared ICC and QUAL using both flat and curved surface elements, and also, the number of surface elements (tiles) and the number of subdivisions

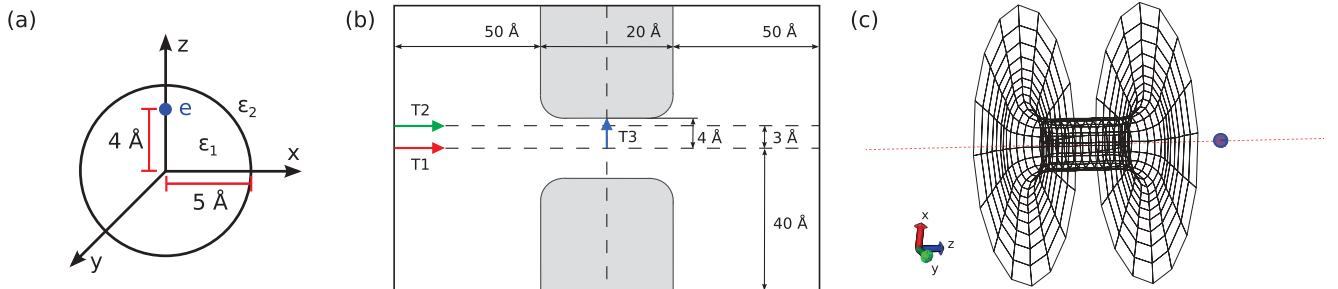


FIG. 1. (Color online) (a) Sphere test case (a). A dielectric sphere of radius  $5 \text{ \AA}$  is embedded in a different dielectric medium. An elementary point charge is set  $4 \text{ \AA}$  off sphere center. (b, c) Ion-channel test case. The model is obtained by rotating (b) by  $180^\circ$  around the axis. The water and the membrane feature different dielectric constants ( $\epsilon_w = 80$  and  $\epsilon_M = 2$ , respectively). The trajectories used for comparison tests are noted in (b) with the labels T1 (along the channel axis), T2 ( $3 \text{ \AA}$  off the channel axis), and T3 (radial direction from the channel axis at the center of the channel). (c) 3D model of the channel. The filled (blue) circle at the right represents the ion moving on the channel axis (red line).

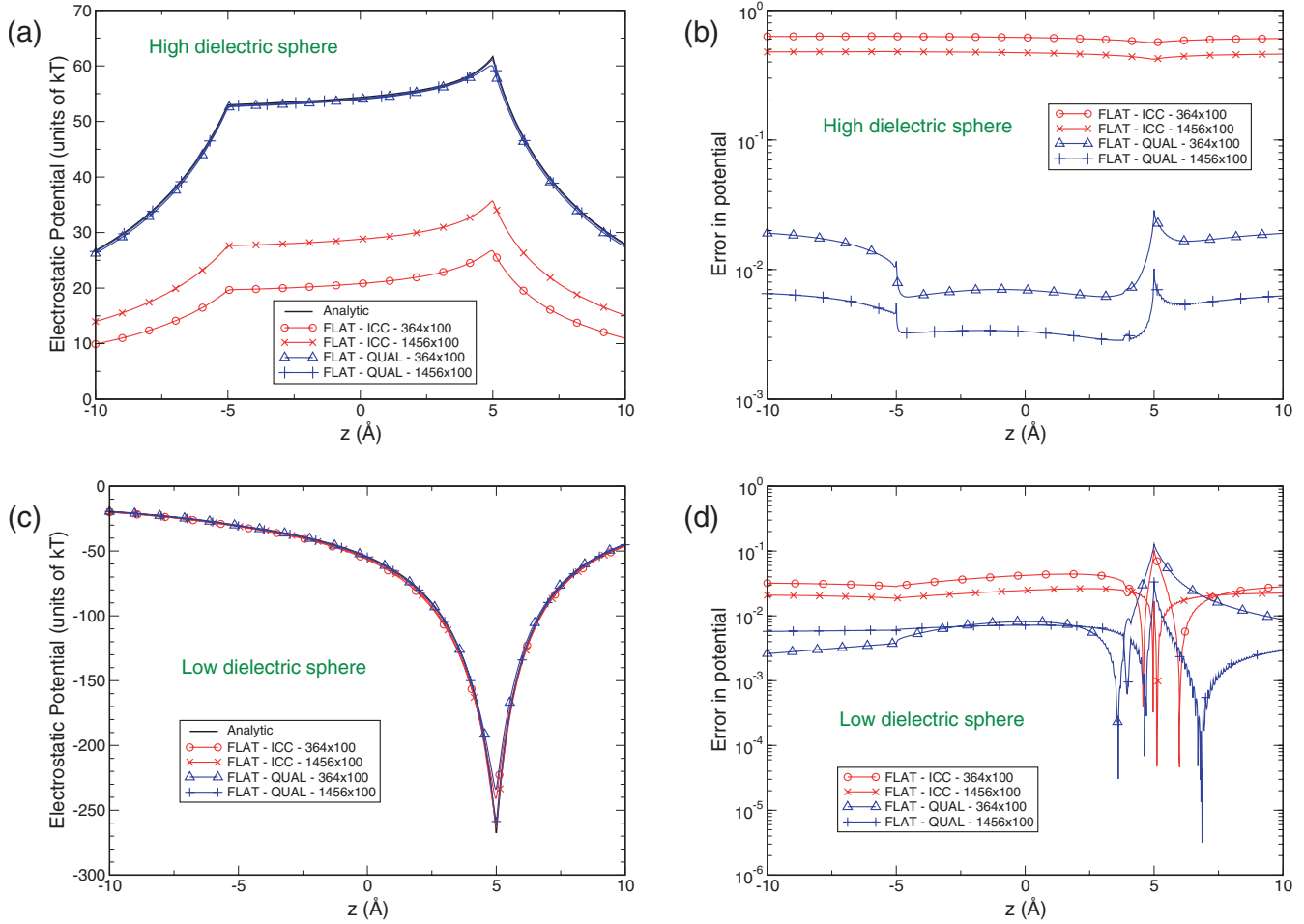


FIG. 2. (Color online) Sphere test cases with flat tiles. Reaction potential and its relative error along the sphere diameter that passes through the source charge (a, b) for the high-dielectric sphere and (c, d) for the low-dielectric sphere. The sphere goes from  $z = -5$  Å to  $z = 5$  Å. The source charge is located at  $z = 4$  Å. In this the subsequent figures, for each data curve, legends give the kind of tiles (flat or curved), the BEM implementation (ICC or QUAL), and the number of tiles and subtiles per tile used to discretize the dielectric boundary (e.g.,  $364 \times 100$  stands for 364 tiles, 100 subtiles for each tile).

of each element (subtiles) were changed to investigate how these parameters affect the accuracy of both methods. In the following figures, each set of data is identified in the captions by the kind of tiles (flat or curved), the BEM implementation (ICC or QUAL), and the number of tiles and subtiles per tile used to discretize the dielectric boundary (e.g.,  $364 \times 100$  means that we used 364 tiles, subdivided into 100 subtiles each for integration).

### A. Dielectric sphere with flat tiles

Our comparison starts with the problem studied by Boda *et al.* [67] and Bardhan *et al.* [71] [Fig. 1(a)]. A spherical dielectric region ( $\epsilon_1$ ) of 5-Å radius is embedded in a different dielectric medium ( $\epsilon_2$ ) and contains an elementary point charge 4 Å away from the center. For the flat-element calculations, the spherical boundary is approximated as a number of flat triangular tiles using spherical coordinates, and then each tile is subdivided into a number of subtiles (16, 36, 64, 100, 144, and 196 in our comparison). Figure 2 shows the reaction potential profiles along the sphere diameter passing through the source

charge, as well as the relative error compared to the analytic solution; we used analytic results computed from [61], but the solution itself is derived in multiple places, e.g., Refs. [94] and [95]. Results for different numbers of tiles used to discretize the dielectric boundary are shown; the plotted results employed 100 subtiles per tile, and results for other numbers of subtiles were not meaningfully different (data not shown).

For the high-dielectric sphere ( $\epsilon_1 = 80$ ) embedded in a low-dielectric medium ( $\epsilon_2 = 2$ ) [Figs. 2(a) and 2(b)], QUAL is noticeably more accurate than ICC for any given number of tiles; in fact, QUAL provides results that are essentially indistinguishable from the analytical result. Figure 2(a) shows that for a high-dielectric sphere with flat tiles, ICC is unable to give satisfactory results even for a large number of tiles. The relative error in reaction potential [Fig. 2(b)] is more than 40% for 1456 tiles and approximately 60% for 384 tiles. For QUAL, however, the relative error in the reaction potential is approximately 3% for the small number of tiles and well under 1% for the large number of tiles. The relative error for QUAL shows a maximum at 5 Å, i.e., at the dielectric boundary, where the accurate evaluation of the

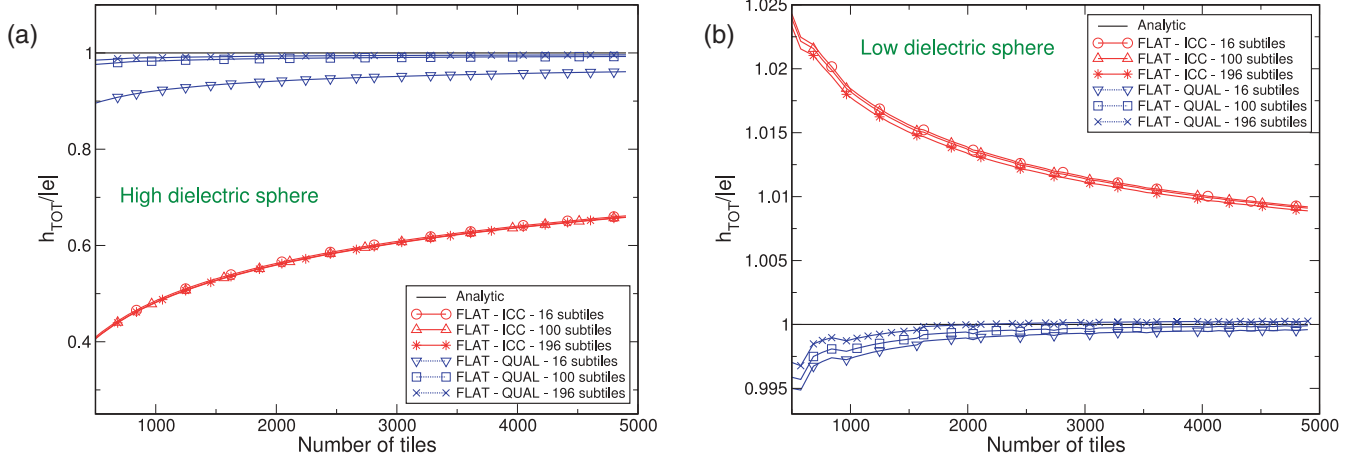


FIG. 3. (Color online) Sphere test cases, flat tiles. Gauss's Law consistency check (a) for the high-dielectric sphere and (b) for the low-dielectric sphere. Graphs show the total induced charge on the boundary, expressed in elementary charge units ( $h_{\text{tot}}/|e|$ ), as a function of the number of tiles used to discretize the dielectric boundary. The number of subtiles per tile is varied.

potential becomes computationally more difficult. Even with the increase in relative error there, however, QUAL is still much more accurate than ICC. Our results correspond very closely to those obtained by Bardhan *et al.* [71], which helps to validate the present implementation. For the low-dielectric sphere ( $\epsilon_1 = 2$ ) in a high-dielectric medium ( $\epsilon_2 = 80$ ), the difference between the two methods is much smaller [Figs. 2(c) and 2(d)]. QUAL still works slightly better almost everywhere, except for the error peak at  $5 \text{ \AA}$ , but both methods provide accuracy to a fraction of  $k_B T$  even for a small number of tiles.

These results agree with other publications demonstrating that a charge in a high-dielectric region is more challenging to compute accurately than a charge in a low-dielectric one [74,80]. Greengard and Lee presented a detailed analysis and discussion, showing that discretization errors have an increasingly large effect on accuracy as the dielectric constant for the charge-containing region increases [80]. Intuitively, it is impossible to have a charge residing in the interior of a conductor rather than on its surface; increasing the dielectric constant in this region makes the problem “closer” to the unphysical limit and is, thus, harder to solve accurately. More precisely, the ICC equation is singular for a conductor [74,80], and Bardhan *et al.* showed that both ICC and QUAL matrices are increasingly ill conditioned as the dielectric constant increases [74].

From Gauss's identity and sum rule, we must have  $h_{\text{tot}}/e = 1$  ( $e$  is the fundamental charge), the total charge inside the sphere. Figure 3 shows the total induced charge computed with the two methods as a function of the number of flat triangular tiles  $N$  used to discretize the sphere surface for the high-dielectric sphere [Fig. 3(a)] and the low-dielectric sphere [Fig. 3(b)]. Each curve represents a different configuration in terms of number of subtiles (16, 100, and 196) used to integrate over each tile. The total charge computed numerically tends to approach the analytical solution as the number of tiles increases. In both cases QUAL features a high consistency even for a low number of tiles. ICC is unable to satisfy Gauss's Law accurately for the high-dielectric sphere since the total induced charge on the boundary is limited to  $\sim 70\%$

of the analytic value. This problem is reduced significantly for the low-dielectric sphere. It is worth noting that, for a given number of tiles, only QUAL is sensitive to the number of subtiles. For QUAL, the dominant error is in the actual panel integration (over the destination panel) rather than the one-point quadrature; in contrast, the dominant error in ICC is the one-point quadrature [71].

## B. Dielectric sphere with curved tiles

We now consider boundaries discretized using curved tiles. For the sphere problems, these tiles were generated by dividing the spherical angles  $\theta$  and  $\phi$  uniformly. An analytic description of the curvature of the dielectric boundary can greatly improve the accuracy of the BEM solutions because tile curvature determines a self-induced contribution that is crucial for the computation of the induced charges. Figure 4 shows the results for the reaction potential and the relative error in reaction potential with respect to the analytic solution along the sphere diameter passing through the source charge and should be compared with the flat-panel results in Fig. 2. Results for different numbers of tiles used to discretize the dielectric boundary are shown. Again, each curved tile is subdivided into 100 curved subtiles, and similar results are obtained using different numbers of subtiles. In this case, for both high-dielectric [Fig. 4(a)] and low-dielectric [Fig. 4(c)] spheres, the ICC and QUAL methods give essentially the same results, with a maximum deviation from analytic results limited to  $0.8 k_B T$ . One can observe the same decrease in relative error as the number of tiles increases. In fact, ICC and QUAL produce almost the same relative errors for both high-permittivity [Fig. 4(b)] and low-permittivity spheres [Fig. 4(d)]. ICC produces marginally smaller errors only for the high-permittivity sphere and large number of tiles.

Figure 5 plots the Gauss's Law consistency check for the high-permittivity [Fig. 5(a)] and low-permittivity [Fig. 5(b)] sphere cases. The total charge induced on the boundary is plotted as a function of the number of tiles and the results are grouped by the number of subtiles used to divide each tile.

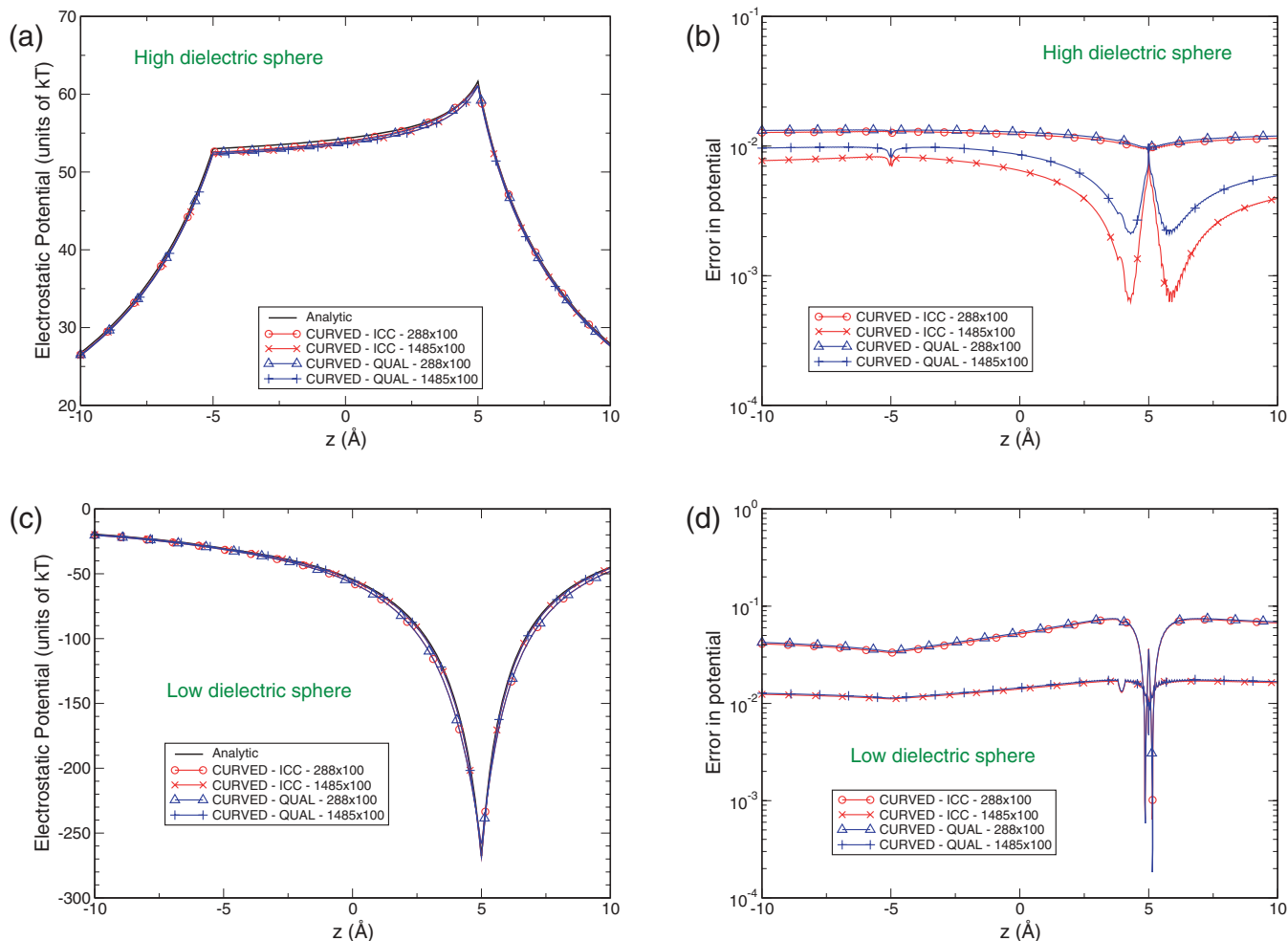


FIG. 4. (Color online) Sphere test cases with curved tiles. Reaction potential and its relative error along the sphere diameter that contains the source charge (a, b) for the high-dielectric sphere and (c, d) for the low-dielectric sphere. Results for both ICC and QUAL were obtained using different numbers of tiles. The sphere goes from  $z = -5 \text{ \AA}$  to  $z = 5 \text{ \AA}$ . The source charge is located at  $z = 4 \text{ \AA}$ .

As expected, in both cases, an increase in the number of tiles produces better estimates of the induced charge. Moreover,

an increase in the number of subtiles per tile helps to satisfy Gauss's identity and sum rule. Again, the low-permittivity

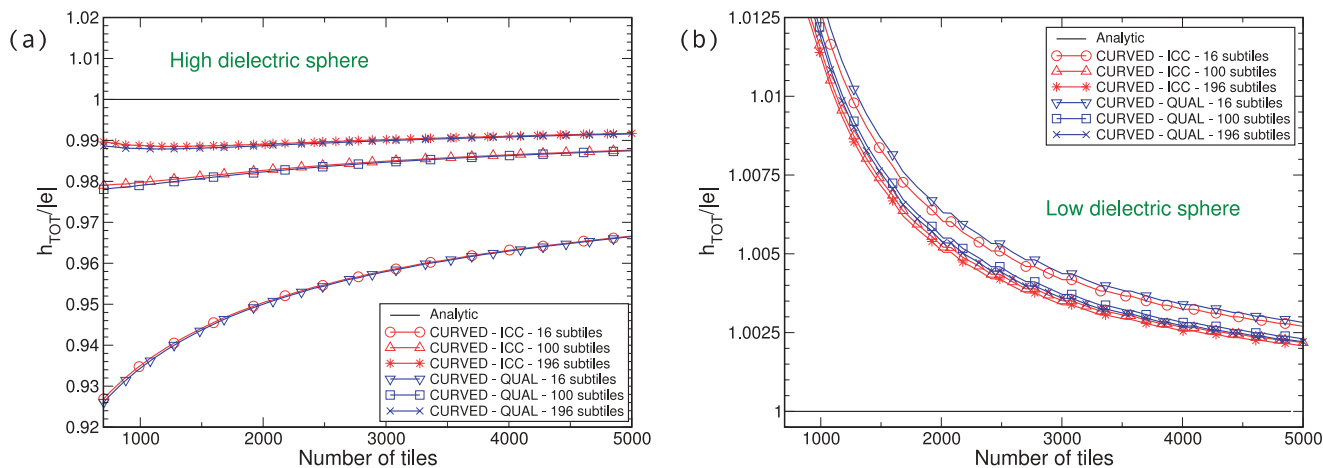


FIG. 5. (Color online) Sphere test cases with curved tiles. Gauss's Law consistency check (a) for the high-dielectric sphere and (b) for the low-dielectric sphere. Graphs show  $h_{tot}$  as a function of the number of tiles used to discretize the dielectric boundary. The number of subtiles per tile is indicated for each curve.

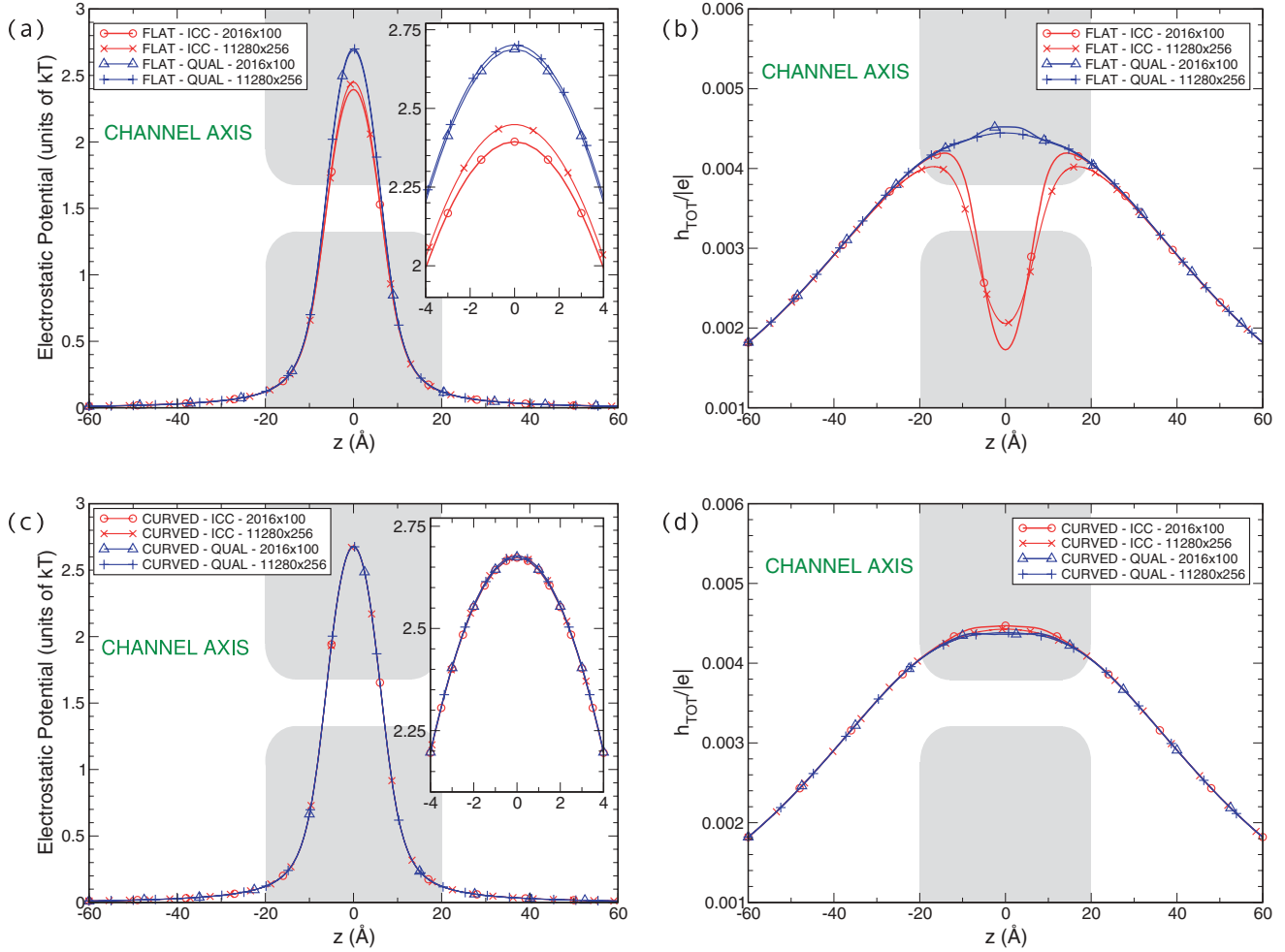


FIG. 6. (Color online) Ion-channel test case for trajectory T1. Reaction potential and  $h_{\text{tot}}$  as a function of the position of a cation that moves along the channel axis (T1). (a, b) Flat and (c, d) curved tiles are used. Results for both ICC and QUAL were obtained using different numbers of tiles and subtiles.

sphere lends itself to improved accuracy, with a minimum error of  $\sim 2.5 \times 10^{-3}$  with respect to  $\sim 1 \times 10^{-2}$  for the high-permittivity sphere case. It is worth noting the different behavior of the two graphs: while in the high-dielectric sphere case the total induced charge underestimates the enclosed charge, in the low-permittivity sphere case both methods overestimate the value of the total induced charge.

### C. Model of an ion channel

In this section we compare the ICC and QUAL implementations using a simple ion-channel model in order to investigate which method is best for studying ion permeation through membrane pores. The ion-channel model is a solid obtained by rotating the shape in Fig. 1(b) around its rotational symmetry axis. The resulting three-dimensional (3D) channel is depicted in Fig. 1(c). A 20-Å-thick membrane slab ( $\epsilon_M = 2$ ) separates two aqueous baths ( $\epsilon_W = 80$ ). A pore with a 4-Å radius connects the two baths. No charges are inserted in the membrane or in the baths and no applied external electric fields are present in the system.

We investigate the accuracy of ICC and QUAL as a cation moves following three different trajectories: (a) along the

channel axis [T1 in Fig. 1(b)]; (b) 3 Å off the channel axis [T2 in Figs. 1(b)]; and (c) in the radial direction, starting from the channel axis at the center of the pore [T3 in Fig. 1(b)]. For each trajectory, we studied the reaction potential felt by the ion and the total induced charge on the dielectric boundary using both flat and curved tiles. Plots were obtained moving the ion in steps of 0.5 Å, solving Poisson's equation with ICC and QUAL, and evaluating the reaction potential at the ion position and the total induced charge on the boundary. The matrix  $\mathbf{A}$  never changes throughout this process, since the geometry of the boundary is fixed. Thus, in BD or in MC simulations, we can compute  $\mathbf{A}$  and its factorization as  $\mathbf{A} = \mathbf{L}\mathbf{U}$  just once, at the beginning of the computation [67]. For any different charge configuration (i.e., as the ion changes its position), we only compute a new right-hand-side  $\mathbf{b}$  and then solve the linear system for the new  $\mathbf{h}$ . The ion, embedded in the high-dielectric water, induces a charge of the same sign on the water-membrane dielectric boundary. The reaction potential increases as the ion approaches the boundary. When the ion crosses the channel along its axis (trajectory T1), the reaction potential felt by the ion increases, reaching its maximum at the channel center [31,96,97].

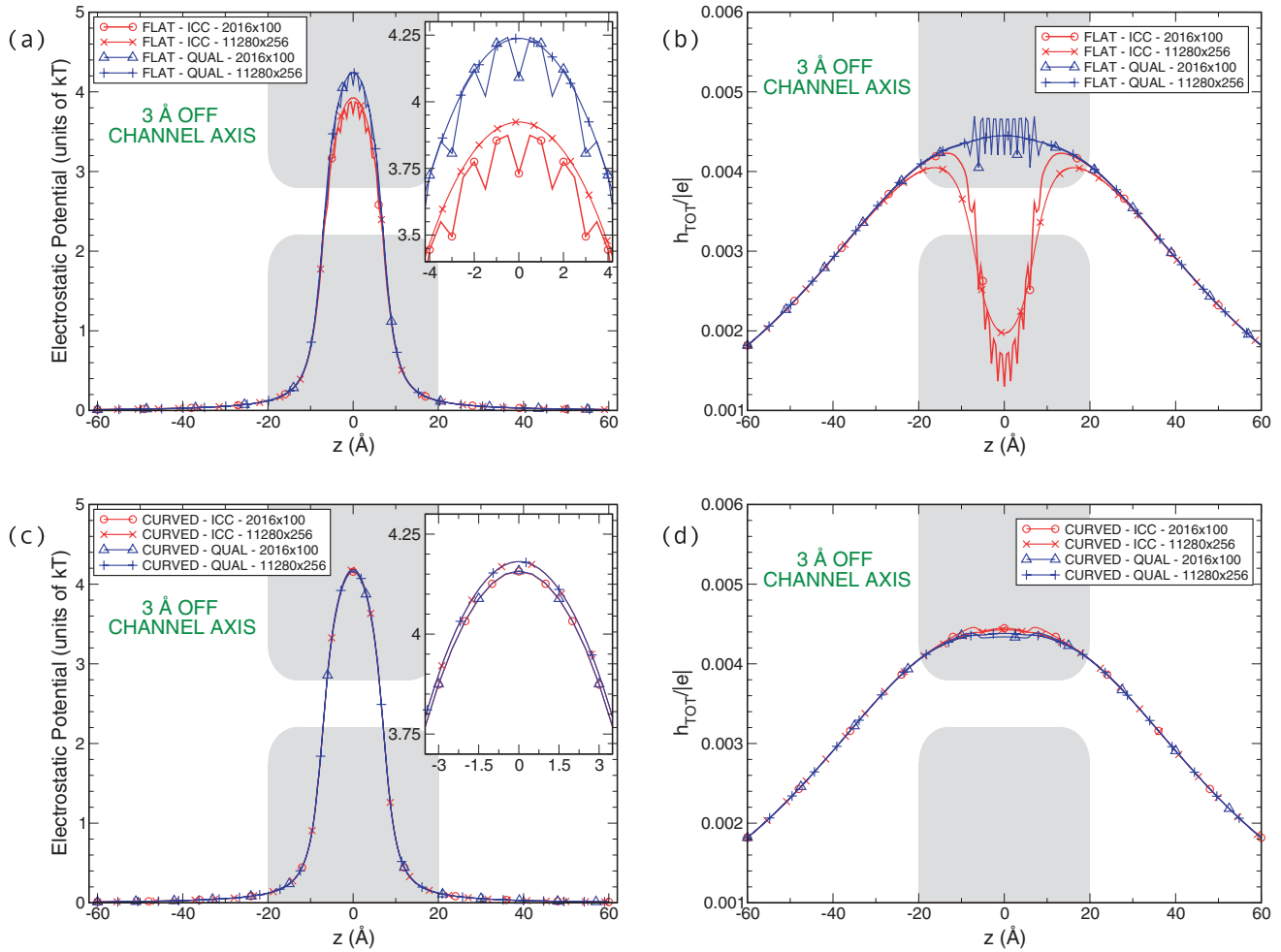


FIG. 7. (Color online) Ion-channel test case for trajectory T2. Reaction potential and  $h_{\text{tot}}$  as a function of the position of a cation that moves 3 Å off the channel axis (T2). (a, b) Flat and (c, d) curved tiles. Results for both ICC and QUAL were obtained using different numbers of tiles and subtiles.

Figure 6 shows results for the reaction potential and sum rule as a cation moves along T1 computed with ICC and QUAL with flat and curved tiles. In this and in the following comparisons, the number of tiles and subtiles have been varied to investigate how finer discretizations can enhance accuracy. For each plot we give the results for a “coarse” discretization (2016 tiles and 100 subtiles per tile) and a “fine” discretization (11 280 tiles and 256 subtiles per tile).

As expected, using flat tiles, ICC exhibits a stronger dependency on the number of discretization elements than does QUAL [Fig. 6(a), including inset]. Unlike the sphere test cases, it is not possible to obtain an analytical solution of this problem, even if the shape of the channel is very simple. Because QUAL exhibited a higher accuracy in the sphere test cases, and also because a refinement of the boundary discretization moves the ICC results toward the QUAL solution, we expect that the “reference solution” of the problem is very close to the “fine” QUAL results. It is worth noting that ICC is quite far from the QUAL curves, even when using a large number of tiles.

For the sum rule, the total charge induced on the boundary must equal the total charge enclosed by the boundary, which

is 0 for our ion-channel model. Figure 6(b) shows the total induced charge as a function of the position of the ion. All implementations feature a high accuracy, limiting the total induced charge to  $5 \times 10^{-3}$  elementary charges. QUAL shows a small dependence on the number of discretization elements. Surprisingly, ICC produces slightly smaller errors in the consistency check as the ion approaches the channel center, even though the ICC calculation accuracy is poorer [Fig. 6(a)]. This result is unexpected because the ICC method exhibited larger sum-rule violations for the sphere examples. More detailed analysis of this discrepancy is needed, but two recent studies suggest ways to eliminate this inaccuracy. Greengard and Lee proposed a modified ICC which improves the accuracy by explicitly enforcing the sum rule [80]. Steinbach *et al.* indicate that eliminating these flat-panel BEM errors requires alternative integral-equation formulations [98]. In that work, the authors use the magnetostatic equivalent of the electrostatic problem studied here and show that flat-tile BEM for the ICC approach gives inaccurate results on the boundary, even when one uses a full Galerkin discretization. As discussed in Sec. II, ICC and QUAL only approximate Galerkin and, thus, cannot be expected to attain even the limited accuracy for surface

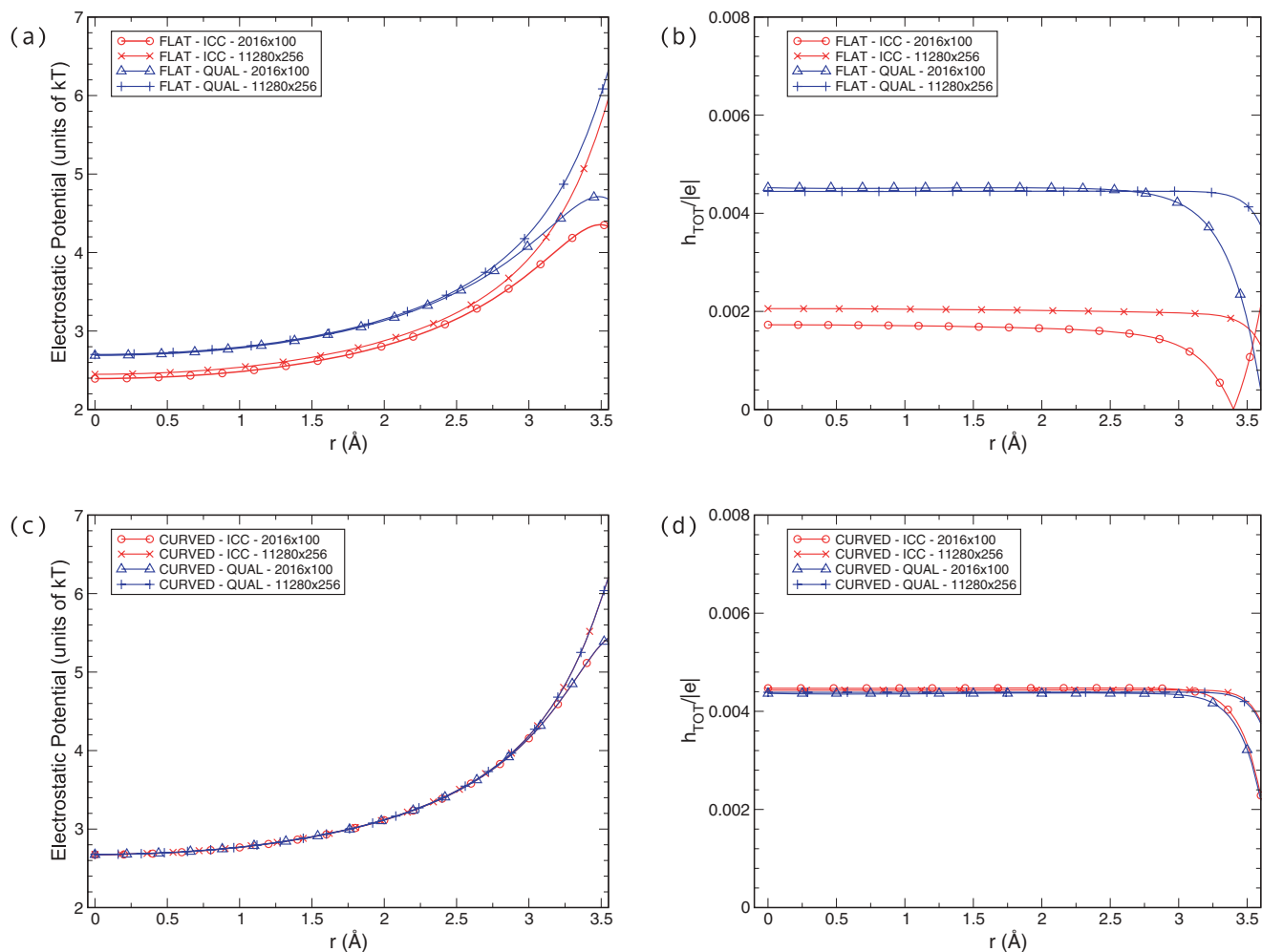


FIG. 8. (Color online) Ion-channel test case for trajectory T3. Reaction potential and  $h_{\text{tot}}$  as a function of the position of a cation that moves radially from the channel axis at the center of the channel (T3). (a, b) Flat and (c, d) curved tiles. Results for both ICC and QUAL were obtained using different numbers of tiles and subtiles.

variables observed there. We intend to test their formulations in future work.

Nevertheless, Fig. 6(b) does serve as a clear example that checking discretization error using the Gauss's Law sum rule is inadequate as the ultimate check for the accuracy of a Poisson solver, because an induced charge  $\mathbf{h}$  that satisfies Gauss's Law does not necessarily give the correct solution to Poisson's equation for the given fixed charge distribution. A useful interpretation of the sum rule is that it verifies the "monopole." Clearly, the fact that an induced-charge distribution satisfies this constraint does not mean that it reproduces all other multipoles. When curved tiles are used to simulate this problem [Fig. 6(c)], ICC and QUAL are basically equivalent as found earlier, producing indistinguishable results for both low and high mesh quality in terms of both reaction potential [Fig. 6(c)] and total induced charge [Fig. 6(d)].

When the ion moves along trajectory T2, 3 Å off the channel axis, it is very close to the dielectric boundary. This means that the computation of the electrostatic forces becomes more critical since polarization charges become larger. In this more demanding test case, using flat tiles [Figs. 7(a) and 7(b)],

a coarse discretization of the boundary leads to a loss of accuracy for both ICC and QUAL. Again, QUAL features a smaller dependence on the number of tiles and ICC still underestimates the reference calculation (i.e., QUAL with a large number of tiles). In this case, as well as for trajectory T1, the total induced charge on the boundary is limited to  $5 \times 10^{-3}$  elementary charges for any configuration. The use of curved tiles [Figs. 7(c) and 7(d)] helps both ICC and QUAL to preserve the accuracy of the solution. The inset in Fig. 7(c) shows how the two methods provide the same results for the same number of tiles. It is important to note that the results for 11 280 flat and curved panels are still different even for QUAL. Since curved panels include curvature better, this shows that curved tiles give more accurate results even for QUAL.

The final comparison is for trajectory T3, in which the ion moves in the radial direction from the channel axis at the center of the channel. Along this path, the ion feels an increasing reaction potential that repels the ion away from the boundary [96]. Figures 8(a) and 8(b) show the reaction potential and the total induced charge on the dielectric boundary as functions of the position of the ion along T3 when flat tiles are adopted.

Both ICC and QUAL feature a clear dependence on the quality of the discretization for distances from the channel axis larger than 2.75 Å. For a given mesh quality, the trend of the plots of ICC and QUAL is functionally indistinguishable, but as in the previous comparisons, ICC never approaches QUAL results, even using a large number of flat discretization elements. Again, the discretization error in Gauss's Law sum rule is smaller for the ICC method than for QUAL, though the magnitude is small, approximately  $5 \times 10^{-3}$  elementary charges.

Finally, we compare using curved tiles to evaluate the electrostatics along T3 [Figs. 8(c) and 8(d)]. Again, for curved tiles ICC and QUAL are equivalent, giving indistinguishable results for the same mesh configuration. Note that the dependence on the number of curved discretization elements is always negligible, with the exception for distances from the channel axis larger than 3.25 Å. In other words, a coarse-grained discretization of the dielectric boundary can provide highly accurate solutions in the whole channel except for less than 1 Å from the boundary. BD and MC simulations often treat ions as hard spheres (their Pauling radii is typically  $\sim 1$  Å [33,67,68,99,100] that cannot cross the dielectric boundaries, so an ion cannot be within  $\sim 1$  Å of the boundary. This dependence is slightly larger, for amplitude and distance, for flat tiles. This means that, using curved tiles, both ICC and QUAL can be adopted to accurately evaluate electrostatics inside an ion channel, even with a surprisingly coarse discretization of the boundary.

#### IV. CONCLUSION

This extensive series of comparisons shows that QUAL is able to provide accurate results using both flat and curved tiles. In contrast, the ICC collocation method produces high-accuracy results only if curved tiles are adopted, in accordance with the hypothesis advanced in earlier work [73]. In fact,

for curved-tile simulations the ICC and QUAL are essentially equivalent in terms of accuracy and speed. Thus, when the dielectric boundary can be described using curved surface elements, both methods can be adopted for particle-based applications.

However, if the dielectric boundary's complexity makes curved tiles impractical and flat tiles must be used, QUAL is significantly more accurate than collocation. Our findings are consistent with earlier results, which indicated that QUAL is usually an order of magnitude more accurate almost everywhere [Fig. 2(d)]. We wish to stress this point and caution the reader that, even though absolute errors appear small [Fig. 2(c)], flat-tile ICC simulations of proteins or other large problems containing hundreds or thousands of charges can have extremely large errors (cf. Fig. 4 of Ref. [83]). Furthermore, the accuracy of the ICC method improves much more slowly than does QUAL when one increases the number of tiles (i.e., ICC converges more slowly). The discretizations of 364 and 1456 elements correspond to vertex densities of approximately 1 and 3 vertices per Å, which are 5–10 times lower than the density required to converge a protein electrostatic free energy. Memory becomes a limiting factor very quickly for the dense BEM employed here, and thus accuracy considerations argue for the use of QUAL for all flat-tile calculations. Even if memory is not a concern, we note that for a given level of accuracy, flat-tile QUAL will be faster than flat-tile ICC, because fewer tiles are needed. Finally, we note that modeling protein-solvent boundaries using atomistic models leads to complicated dielectric interfaces and curved-tile surface representations are difficult to obtain, e.g., Refs. [75–77,101]. However, as argued by Steinbach *et al.* [98], important properties of the integral operators depend quite sensitively on the smoothness of the actual surface representation; thus, when flat panels must be used, alternative integral equations may be valuable for fast and accurate simulations.

- 
- [1] W. R. Fawcett, *Liquids, Solutions, and Interfaces: From Classical Macroscopic Descriptions to Modern Microscopic Details* (Oxford University Press, New York, 2004).
  - [2] K. J. Laidler and J. H. Meiser, *Physical Chemistry, Vol. 1.* (Houghton Mifflin, Boston, 1999).
  - [3] J. Vincze, M. Valisko, and D. Boda, *J. Chem. Phys.* **133**, 154507 (2010).
  - [4] J. Barker and D. Henderson, *Rev. Mod. Phys.* **48**, 587 (1976).
  - [5] C. A. Barlow Jr. and J. R. Macdonald, *Theory of Discreteness of Charge Effects in the Electrolyte Compact Double Layer* (Interscience, New York, (1967), pp. 1–199).
  - [6] D. Gillespie, W. Nonner, and R. S. Eisenberg, *J. Phys.: Condens. Matter* **14**, 12129 (2002).
  - [7] J. P. Hansen and I. R. McDonald, *Theory of Simple Liquids* (Academic Press, San Diego, CA, 2006).
  - [8] B. Roux and T. Simonson, *Biophys. Chem.* **78**, 1 (1999).
  - [9] M. Z. Bazant, K. Thornton, and A. Ajdari, *Phys. Rev. E* **70**, 021506, (2004).
  - [10] Y. Hyon, J. E. Fonseca, B. Eisenberg, and C. Liu (in press, 2012).
  - [11] M. Valiskó, D. Boda, and D. Gillespie, *J. Phys. Chem. C* **111**, 15575 (2007).
  - [12] B. Roux, B. Prod'hom, and M. Karplus, *Biophys. J.* **68**, 876 (1995).
  - [13] K. A. Sharp and B. Honig, *Annu. Rev. Biophys. Biophys. Chem.* **19**, 301 (1990).
  - [14] Z. Chen, N. A. Baker, and G. W. Wei, *J. Comput. Phys.* **229**, 8231 (2010).
  - [15] Z. Chen, N. A. Baker, and G. W. Wei, *J. Math. Biol.* **63**, 1139 (2011).
  - [16] B. Li, *Nonlinearity* **22**, 811 (2009).
  - [17] B. Li, *SIAM J. Math. Anal.* **40**, 2536 (2009).
  - [18] M. Lundstrom, *Fundamentals of Carrier Transport* (Cambridge University Press, Cambridge, 2009).
  - [19] P. A. Markowich, C. A. Ringhofer, and C. Schmeiser, *Semiconductor Equations* (Springer-Verlag, New York, 1990).
  - [20] B. Eisenberg, *Fluctuat. Noise Lett.* **11**, 76 (2012). [Earlier version, Living Transistors: A Physicist's View of Ion Channels, available at <http://arxiv.org/abs/0506016v0506012>.]

- [21] G. Baccarani, M. Rudan, M. Lorenzini, W. Fichtner, J. Litsios, A. Schenk, P. van Staa, L. Kaeser, A. Kampmann, A. Marmiroli, C. Sala, and E. Ravanelli, in *Electronics, Circuits, and Systems (1996). ICECS '96, Proceedings of the Third IEEE International Conference, Vol. 2* (IEEE, New York, 1996), pp. 752–755.
- [22] I. Avci, P. Balasingam, K. E. Sayed, J. Gharib, M. D. Johnson, K. Kells, G. Kiralyfalvi, V. Kolyzhenkov, A. Kucherov, E. Lyumkis, O. Penzin, B. Polsky, V. Rao, S. D. Simeonov, N. Strecker, Z. Tan, L. Villablanca, and W. Fichtner, in *University/Government/Industry Microelectronics Symposium, 2006 16th Biennial*, San Jose State University, San Jose, CA, June 25–28 (2006).
- [23] M. Braccioli, G. Curatola, Y. Yang, E. Sangiorgi, and C. Fiegna, in *Ultimate Integration of Silicon, 2008, ULIS 2008, 9th International Conference* (2008), p. 71.
- [24] C. Jacoboni and P. Lugli, *The Method for Semiconductor Device Simulation* (Springer-Verlag, New York, 1989).
- [25] J. Tomasi and M. Persico, *Chem. Rev.* **94**, 2027 (1994).
- [26] B. Honig and A. Nicholls, *Science* **268**, 1144 (1995).
- [27] F. B. Sheinerman, R. Norel, and B. Honig, *Curr. Opin. Struct. Biol.* **10**, 153 (2000).
- [28] S. H. Northrup and H. P. Erickson, *Proc. Natl. Acad. Sci. USA* **89**, 3338 (1992).
- [29] D. P. Tieleman, P. C. Biggin, G. R. Smith, and M. S. P. Sansom, *Q. Rev. Biophys.* **34**, 473 (2001).
- [30] D. G. Levitt, *Biophys. J.* **22**, 209 (1978).
- [31] P. C. Jordan, *Biophys. J.* **39**, 157 (1982).
- [32] S.-H. Chung, M. Hoyles, T. Allen, and S. Kuyucak, *Biophys. J.* **75**, 793 (1998).
- [33] Matthew Hoyles, Serdar Kuyucak, and Shin-Ho Chung, *Phys. Rev. E* **58**, 3654 (1998).
- [34] M. Nina, D. Beglov, and B. Roux, *J. Phys. Chem. B* **101**, 5239 (1997).
- [35] W. Im and B. Roux, *J. Chem. Phys.* **115**, 4850 (2001).
- [36] W. Nonner, L. Catacuzzeno, and B. Eisenberg, *Biophys. J.* **79**, 1976 (2000).
- [37] Z. Schuss, B. Nadler, and R. S. Eisenberg, *Phys. Rev. E* **64**, 036116 (2001).
- [38] B. Nadler, U. Hollerbach, and R. S. Eisenberg, *Phys. Rev. E* **68**, 021905 (2003).
- [39] T. Baštuž and S. Kuyucak, *Biophys. J.* **84**, 2871 (2003).
- [40] R. D. Coalson and M. G. Kurnikova, *IEEE Trans. NanoBiosci.* **4**, 81 (2005).
- [41] J. Stenhammar, M. Trulsson, and P. Linse, *J. Chem. Phys.* **134**, 224104 (2011).
- [42] H. Wang, F. Dommert, and C. Holm, *J. Chem. Phys.* **133**, 034117 (2010).
- [43] R. Zhou, E. Harder, H. Xu, and B. J. Berne, *J. Chem. Phys.* **115**, 2348 (2001).
- [44] J. Warwicker and H. C. Watson, *J. Mol. Biol.* **157**, 671 (1982).
- [45] J. Lacombe, K. Chakanga, S. Geissendörfer, K. Von Maydell, and C. Agert, in *Proceedings of 35th IEEE Photovoltaic Specialists Conference (PVSC), 2010 Honolulu, HI* (IEEE, New York, 2010), p. 001535.
- [46] M. K. Gilson, A. Rashin, R. Fine, and B. Honig, *J. Mol. Biol.* **184**, 503 (1985).
- [47] M. E. Davis and J. A. McCammon, *J. Comput. Chem.* **10**, 386 (1989).
- [48] A. Nicholls and B. Honig, *J. Comput. Chem.* **12**, 435 (1991).
- [49] U. A. Ranawake, C. Huster, P. M. Lenders, and S. M. Goodnick, *IEEE Trans. Comput. Aided Design Integr. Circ. Syst.* **13**, 712 (1994).
- [50] A. Wexler and D. J. Richards, in *Microwave Symposium Digest, 1971 IEEE GMITT International, Washington, DC* (IEEE, New York, 1971), p. 132.
- [51] P. P. Silvester and D. Omeragic, *IEEE Trans. Magnet.* **29**, 1993 (1993).
- [52] N. A. Baker, D. Sept, M. J. Holst, and J. A. McCammon, *Proc. Natl. Acad. Sci. USA* **98**, 10037 (2001).
- [53] S. Coco, D. S. M. Gazzo, A. Laudani, and G. Pollicino, in *Proceedings of 12th Biennial IEEE Conference on Electromagnetic Field Computation, Miami, FL* (IEEE, New York, 2006), p. 277.
- [54] S. Rush, A. H. Turner, and A. H. Cherin, *J. Appl. Phys.* **37**, 2211 (1966).
- [55] B. H. McDonald, M. Friedman, and A. Wexler, *IEEE Trans. Microwave Theory* **22**, 237 (1974).
- [56] T. Sometani and K. Hasebe, *Am. J. Phys.* **45**, 918 (1977).
- [57] S. Miertus, E. Scrocco, and J. Tomasi, *Chem. Phys.* **55**, 117 (1981).
- [58] R. J. Zauhar and R. S. Morgan, *J. Mol. Biol.* **186**, 815 (1985).
- [59] P. B. Shaw, *Phys. Rev. A* **32**, 2476 (1985).
- [60] A. A. Rashin, *J. Phys. Chem.* **94**, 1725 (1990).
- [61] D. Boda, D. Gillespie, W. Nonner, D. Henderson, and B. Eisenberg, *Phys. Rev. E* **69**, 046702 (2004).
- [62] Z. Xu and W. E. I. Cai, *Direct* **53**, 683 (2011).
- [63] B. Toland, B. Houshmand, and T. Itoh, *IEEE Microwave Guided Wave Lett.* **3**, 333 (1993).
- [64] G.-L. Tan, N. Bewtra, K. Lee, and J. M. Xu, *IEEE J. Quantum Electron.* **29**, 822 (1993).
- [65] A. Husain and S. G. Chamberlain, *IEEE J. Solid-State Circ.* **17**, 261 (1982).
- [66] M. Fukuma and R. H. Uebbing, in *Electron Devices Meeting, 1984 International* (IEEE, New York, 1984), Vol. 30, p. 621.
- [67] D. Boda, M. Valiskó, R. S. Eisenberg, W. Nonner, D. Henderson, and D. Gillespie, *J. Chem. Phys.* **125**, 034901 (2006).
- [68] D. Boda, T. Varga, D. Henderson, D. D. Busath, W. Nonner, D. Gillespie, and B. Eisenberg, *Mol. Simul.* **30**, 89 (2004).
- [69] B. J. Yoon and A. M. Lenhoff, *J. Comput. Chem.* **11**, 1080 (1990).
- [70] A. Juffer, E. F. F. Botta, B. A. M. van Keulen, A. van der Ploeg, and H. J. C. Berendsen, *J. Comput. Phys.* **97**, 144 (1991).
- [71] J. P. Bardhan, *J. Chem. Phys.* **130**, 094102 (2009).
- [72] S. Kuyucak, M. Hoyles, and S.-H. Chung, *Biophys. J.* **74**, 22 (1998).
- [73] J. Tausch, J. Wang, and J. K. White, *IEEE Trans. Comput. Aided Design Integr. Circ. Syst.* **20**, 1398 (2001).
- [74] J. P. Bardhan, R. S. Eisenberg, and D. Gillespie, *Phys. Rev. E* **80**, 011906 (2009).
- [75] J. Liang and S. Subramaniam, *Biophys. J.* **73**, 1830 (1997).
- [76] R. J. Zauhar, *J. Comput. Aided Mol. Design* **9**, 149 (1995).
- [77] M. D. Altman, J. P. Bardhan, J. K. White, and B. Tidor, *J. Comput. Chem.* **30**, 132 (2009).
- [78] A. Malasics, D. Boda, M. Valiskó, D. Henderson, and D. Gillespie, *Biochim. Biophys. Acta Biomembranes* **1798**, 2013 (2010).
- [79] D. Boda, W. Nonner, M. Valiskó, D. Henderson, B. Eisenberg, and D. Gillespie, *Biophys. J.* **93**, 1960 (2007).

- [80] L.e Greengard and J.-Y. Lee, *J. Comput. Phys.* **211**, 64 (2006).
- [81] K. E. Atkinson, *The Numerical Solution of Integral Equations of the Second Kind* (Cambridge University Press, Cambridge, 1997).
- [82] K. Nabors and J. White, *IEEE Trans. Comput. Aided Design Integr. Circ. Syst.* **10**, 1447 (1991).
- [83] M. D. Altman, J. P. Bardhan, J. K. White, and B. Tidor, in *Proceedings of 27th Annual International Conference on Engineering in Medicine and Biology Society (EMBS), Shanghai* (IEEE, New York, 2005), p. 7591.
- [84] J. L. Hess and A. M. O. Smith, *J. Ship Res.* **8**, 22 (1962).
- [85] J. N. Newman, *J. Eng. Math.* **20**, 113 (1986).
- [86] J.-L. Guermond, *SIAM J. Numer. Anal.* **29**, 1347 (1992).
- [87] J. P. Bardhan, M. D. Altman, D. J. Willis, S. M. Lippow, B. Tidor, and J. K. White, *J. Chem. Phys.* **127**, 014701 (2007).
- [88] Y. Saad and M. H. Schultz, *J. Sci. Stat. Comput.* **7**, 856 (1986).
- [89] R. Bharadwaj, A. Windemuth, S. Sridharan, B. Honig, and A. Nicholls, *J. Comput. Chem.* **16**, 898 (1995).
- [90] A. H. Boschitsch, M. O. Fenley, and H.-X. Zhou, *J. Phys. Chem. B* **106**, 2741 (2002).
- [91] B. Lu, X. Cheng, J. Huang, and J. Andrew McCammon, *Proc. Natl. Acad. Sci. USA* **103**, 19314 (2006).
- [92] S. S. Kuo, M. D. Altman, J. P. Bardhan, B. Tidor, and J. K. White, in *International Conference on Computer Aided Design (ICCAD)* (IEEE, New York, 2002), p. 466.
- [93] M. D. Altman, J. P. Bardhan, B. Tidor, and J. K. White, *IEEE Trans. Comput. Aided Design Integr. Circ. Syst.* **25**, 274 (2006).
- [94] J. D. Jackson, *Classical Electrodynamics*, 3rd ed. (Wiley, New York, 1998).
- [95] T. P. Doerr and Y.-K. Yu, *Am. J. Phys.* **72**, 190 (2004).
- [96] M. Hoyles, S. Kuyucak, and S.-H. Chung, *Comput. Phys. Commun.* **115**, 45 (1998).
- [97] P. C. Jordan, *Biophys. J.* **45**, 1091 (1984).
- [98] Z. Andjelic, G. Of, O. Steinbach, and P. Urthaler, *Comput. Visual Sci.* **14**, 117 (2011).
- [99] B. Corry, T. W. Allen, S. Kuyucak, and S.-H. Chung, *Biophys. J.* **80**, 195 (2001).
- [100] S.-H. Chung, T. W. Allen, M. Hoyles, and S. Kuyucak, *Biophys. J.* **77**, 2517 (1999).
- [101] A. J. Bordner and G. A. Huber, *J. Comput. Chem.* **24**, 353 (2003).